ChinaRiceCalendar-Seasonal Crop Calendars for Early, Middle, and Late Rice in China

Hui Li[1], Xiaobo Wang[2,*], Shaoqiang Wang[1,2,3,4,*], Yuanyuan Liu[2], Zhenhai Liu[2], Shiliang Chen[1,2], Qinyi Wang[1], Tongtong Zhu[1], Lunche Wang[1], Lizhe Wang[5]

[1]Key Laboratory of Regional Ecology and Environmental Change, School of Geography and Information Engineering, China University of Geosciences, Wuhan, 430074, China

[2]Key Laboratory of Ecosystem Network Observation and Modeling, Institute of Geographic Sciences and Natural Resources Research, CAS, Beijing, 100101, China

[3]State Key Laboratory of Biogeology and Environmental Geology, China University of Geosciences, Wuhan 430074, China;

[4]College of Resources and Environment, University of Chinese Academy of Sciences, Beijing 100049, China;

[5]Hubei Key Laboratory of Intelligent Geo-Information Processing, China University of Geosciences, Wuhan 430074, China

*Correspondence to: Xiaobo Wang (wxbwxb1995@163.com); Shaoqiang Wang (sqwang@igsnrr.ac.cn)

Abstract. Long-time series and large-scale rice calendar datasets provide valuable information for agricultural planning and field management in rice-based cropping systems. However, current regional-level rice calendar datasets do not accurately distinguish between rice seasons in China, causing uncertainty in crop model simulation and climate change impact analysis. Based on satellite remote sensing data and an improved PhenoRice algorithm, we extracted the crop areas and phenology of early-, middle-, and late-season rice across China from 2003 to 2020, and established a multi-season rice calendar dataset named ChinaRiceCalendar. Overall, the ChinaRiceCalendar dataset shows a good agreement not only with field-observed rice calendars in Agricultural Meteorological Stations (AMSs), but also with statistical rice areas in various growing seasons. According to the calendar data from 2003 to 2020, the transplanting dates for early, middle, and late rice shifted by +5.4, +2.6, and -5.7 DOY/decade, respectively; the flowering date for early, middle, and late rice shifted by +5.5, -2.8, and -2.7 DOY/decade, respectively; the maturity date for early, middle, and late rice shifted by +3.2, -3.6, and -5.1 DOY/decade, respectively. The ChinaRiceCalendar can be utilized to investigate and optimize the spatio-temporal structure of rice cultivation in China under climate and land-use change.

1   Introduction

As one of the major food crops, rice feeds nearly half of the world's population (Nelson and Gumma, 2015; Fahad et al., 2019). In the context of climate change, continued warming is projected to result in shorter crop growth periods, lower rice productivity, and food insecurity in the Asian monsoon region (Carleton, 2017; Zhao et al., 2017; IPCC, 2022). Revealing changes in rice phenology will facilitate

timely adjustment of planting time, rice cultivars, and cropping systems under global warming (Waha et al., 2013; Wang et al., 2022; Wang et al., 2024). Moreover, a dynamic rice calendar with key phenological dates is integral to agricultural monitoring and farmer support systems (Laborte et al., 2017; Fritz et al., 2019; Mishra et al., 2021). Large-scale rice calendars can contribute to more reliable simulations of crop growth and yield at regional and global scales (Franke et al., 2020).

Satellite remote sensing is an effective tool for detecting long-term trends in crop phenology at the regional scale (Xiao et al., 2006; Kotsuki and Tanaka, 2015; Luo et al., 2020; Gao and Zhang, 2021; Mishra et al., 2021). Crop phenology detection methods based on remote sensing vegetation indices (VIs) can be categorized into threshold, inflection point, and shape model approaches. The threshold approaches assume that a development stage begins when the VI value exceeds a predefined threshold (Jönsson et al., 2004; Boschetti et al., 2009; Pan et al., 2015; Guo et al., 2016). The inflection point approaches reconstruct the VI time-series curve by filter smoothing or function fitting, and then corresponds the maxima, minima, and inflection points on the curve to the key phenological events (Zhang et al., 2003; Sakamoto et al., 2005; Sun et al., 2009; Wang et al., 2019). The shape model approaches fit observed VI time-series curves by geometric scaling a robust standard VI time-series curve for the specific crop to identify development stages (Sakamoto et al., 2010; More et al., 2016; Zeng et al., 2016; Sakamoto et al., 2018). In addition to the methods based on time series of VIs, there are also rule-based algorithms that integrate multiple approaches and indicators to detect crop phenology, such as the PhenoRice algorithm proposed by Boschetti et al. (2017). The PhenoRice algorithm, which combines the advantages of threshold and inflection point approaches, utilizes the Enhanced Vegetation Index (EVI), the Normalized Difference Flood Index (NDFI), and the land surface temperature (LST) to estimate rice planting dates. The PhenoRice algorithm excels at extracting rice phenology in multiple cropping systems and has been widely used in East Asia, South Asia, Southeast Asia, and Europe (Busetto et al., 2019; Liu et al., 2020; Mishra et al., 2021). However, the performance of the PhenoRice algorithm depends on the division of rice seasons, which requires expert knowledge about rice-based cropping systems in different regions (Mishra et al., 2021).

In China, there are at least three rice-growing seasons (early, middle, and late seasons) in diverse rice-based cropping systems (e.g., single-rice, double-rice, rice-wheat, rice-rapeseed, and rice-vegetable systems) (Frolking et al., 2002; Qiu et al., 2003; Cao et al., 2021; He et al., 2021). Generally, early-, middle-, and late-season rice are transplanted at Day Of Year (DOY) 30-130, DOY 110–180, and DOY 150-230, respectively. The growth periods after transplanting for early, middle, and late rice are 70-100 days, 100-130 days, and more than 130 days, respectively. Although field observations are important data sources for studying rice calendars in different growing seasons, they are usually limited by spatial and temporal discontinuities (Zhao et al., 2016; Wang et al., 2017). Therefore, previous studies have typically utilized satellite remote sensing products to establish rice calendar datasets at the regional scale (Shihua et al., 2014; Liu et al., 2019; Bai and Xiao, 2020; Luo et al., 2020; Mishra et al., 2021). Nevertheless, these calendar datasets based on satellite remote sensing do not rationally classify rice growing seasons across China. For example, the dataset ChinaCropPhen1km only distinguishes between early and late rice in double-rice systems (Luo et al., 2020); the assumptions of the dataset RICA about rice flowering dates in different seasons do not correspond to the realities in China (Mishra et al., 2021); Shen et al. (2023) produced high-resolution distribution maps of single-season rice but did not explore multiple rice cropping systems. Early-,

middle- and late-season rice in China are not only planted at different times, but also have distinguishing varietal characteristics, such as different temperature and photoperiod sensitivities (Zong et al., 2021). Thus, a crop calendar that accurately classifies rice seasons will provide reliable data for agricultural models to calibrate crop parameters at the variety level. Moreover, effective identification of different rice seasons will help analyze the response and adaptation of rice phenology to climate change.

Therefore, to address the shortcomings of the existing rice calendar datasets in China, we attempted to improve the PhenoRice algorithm and use satellite remote sensing data to (1) establish crop calendars for early, middle, and late rice in China; (2) validate the extracted rice areas and calendars in different growing seasons; and (3) explore the spatio-temporal changes of rice calendar dates in major agricultural zones across China from 2003 to 2020.

2 Data and Methodology

2.1 Study area

We selected seven agricultural zones in China as the study area: the Northeast Plain (NP), Huanghuaihai Plain (HP), Loess Plateau (LP), Middle and Lower Yangtze River Region (MLY), South China Region (SC), Yunnan-Guizhou Plateau (YGP), and Sichuan Basin and Surrounding Region (SCS) (Fig. 1). Due to limited hydrothermal resources, the NP and HP zones mainly cultivates single-season rice. Early, middle, and late rice exist in different cropping systems in the MLY zone. The SC zone has a higher cropping frequency than other zones and usually cultivates rice twice a year. Parts of Hainan Province cultivates rice three times a year. Agricultural zoning data were obtained from Resources and Environment Science and Data Center (https://www.resdc.cn/data.aspx?DATAID=275).

2.2 Data

2.2.1 Satellite Imagery

MODIS (Moderate Resolution Imaging Spectroradiometer) remote sensing data are widely used in crop phenology detection because of their excellent performance in temporal and spatial continuity (Reed et al., 1994; Zhang et al., 2003; Zhao et al., 2011; Son et al., 2013). We selected two MODIS EVI products for the study area during 2003–2020: MOD13Q1 (TERRA data) and MYD13Q1 (AQUA data) (https://doi.org/10.5067/MODIS/MOD13Q1.061, 250 m, 16-day). Because the TERRA and AQUA data are based on the synthetic period of moving eight days from each other, the time series of the two 16-day products of MOD13Q1 and MYD13Q1 have a temporal resolution of 8 days (Boschetti et al., 2017). The red (ρ_{RED}) and near-red (ρ_{SWIR}) bands of MOD13Q1 and MYD13Q1 were used to calculate the Normalized Flooding Index (NDFI) (Eq. 1). The Pixel Reliability, Usefulness Index, and Blue Band Reflectance from MOD13Q1/MYD13Q1 were used to assess data quality. In addition, the 1 km spatial resolution and 8-day temporal resolution Land Surface Temperature (LST) product MOD11A2 (https://doi.org/10.5067/MODIS/MOD11A2.061) was employed by resampling 250 m

117 spatial resolution consistent with EVI data.

$$NDFI = \frac{\rho_{RED} - \rho_{SWIR}}{\rho_{RED} + \rho_{SWIR}} \tag{1}$$

119 All time series data were processed through the Google Earth Engine (GEE) platform and the Python
120 package of Geemap (Wu, 2020).

2.2.2 Validation Data

122 We obtained the statistical sown areas of rice at the province level during 2003-2020 from the Chinese
123 Agricultural Yearbooks (https://data.cnki.net/yearBook/single?id=N2020120306). We also collected
124 site-scale observations including rice seasons and key phenological dates (transplanting, flowering, and
125 maturity dates) between 2003 and 2013 from 338 Agricultural Meteorological Stations (AMSs,
126 https://data.cma.cn/) in China. Moreover, we compared ChinaRiceCalendar with other regional-scale
127 calendar datasets, including the RiceAtlas dataset based on the agricultural statistics (Laborte et al.,
128 2017), the ChinaCropPhen1km dataset based on the Global Land Surface Satellite (GLASS) leaf area
129 index (LAI) products (Luo et al., 2020), and the RICA dataset based on the MOD13Q1/MYD13Q1
130 products (Mishra et al., 2021).

2.2.3 Additional Data

132 Cropland data were obtained from the International Geosphere-Biosphere Program (IGBP)
133 classification of the MODIS land cover product (MCD12Q1) from 2003 to 2020
134 (https://doi.org/10.5067/MODIS/MCD12Q1.006). Digital elevation model (DEM) data used to create a
135 terrain mask were obtained from the Shuttle Radar Topography Mission (SRTM,
136 https://srtm.csi.cgiar.org). Both data are resampled to a spatial resolution of 250 m.

2.3 Methodology

138 The technology roadmap of this study is shown in Fig. 2.

2.3.1 Data pre-processing

140 The data pre-processing in the study falls into three steps:

142 1. The signal of agronomic flooding was used to help identify the rice transplanting period, but
143 non-agricultural wetlands may have similar flooding signals to paddy fields (Dong and Xiao,
144 2016; Han et al., 2022). Thus, the annual cropland extent from 2003 to 2020 was used to establish
145 a cropland mask to screen the cropland pixels of the MODIS EVI data.

146 2. Given that too high an elevation or too great a slope is unsuitable for paddy rice cultivation
147 (Gumma et al., 2011; Dong and Xiao, 2016), only the image pixels with an elevation below 2600
148 m and a slope less than 8° were selected to extract rice calendars (Han et al., 2022).

149 3. To reduce the impacts of cloud contamination, we deleted the image pixels with reflectance
150 greater than 0.2 in the blue band (Xiao et al., 2006).

151 **2.3.2 Estimation of rice area and cropping calendar**

152 We combined the PhenoRice algorithm (Boschetti et al., 2017) with a growing season division method
153 (Kong et al., 2022) to extract rice areas and cropping calendars in different growing seasons. Firstly,
154 we identified possible crop flowering periods based on a weighted-smoothed EVI time-series curve in
155 each image pixel. Then we input the possible flowering periods into the PhenoRice algorithm to divide
156 potential growing seasons and check if the corresponding EVI time series belongs to rice. Lastly, we
157 estimated rice planting, flowering, and maturity dates and categorized them into early-, middle-, and
158 late-season calendars according to transplanting time and growing period length.

159 ① **Divide potential growing seasons**: The PhenoRice algorithm requires a pre-specification of rice
160 flowering periods in different growing seasons to extract the corresponding VI time series. To
161 reduce the uncertainty caused by the artificial division of growing seasons, we employed the
162 *phenofit* R package developed by Kong et al. (2022) to identify possible flowering periods in each
163 image pixel. 1) The weighted Whittaker method in the *phenofit* R package was employed to
164 smooth the MODIS-EVI time series (Kong et al., 2022). The Whittaker smoothing function can
165 robustly capture seasonal signals with little noise interference, and it is widely used to identify
166 crop phenology (Atzberger and Eilers, 2011; Bush et al., 2017). The curve fitting mainly relies on
167 information from good-quality points, but also extracts the limited information available from the
168 marginal- and bad-quality points. During the rough fitting to the EVI time series, we categorized
169 the data quality of the observations according to their Quality Control (QC) information
170 (SummaryQA of MOD13A1) and assigned weights of 1.0, 0.5, and 0.2 to the good-, marginal-,
171 and bad-quality VI observations, respectively. 2) Following Kong et al. (2022), the possible
172 flowering date (peak point date) in each crop season was identified by the smoothed EVI time
173 series, based on the rules that only one peak value is inside a growing season and two trough
174 values define a growing season. 3) The possible flowering periods (peak point dates $\pm$ 16 days)
175 detected in each image pixel were input into the PhenoRice algorithm to generate the potential
176 growing seasons.

177 ② **Check if the pixel belongs to a rice-cultivated area**: Whether the pixel belongs to a rice-
178 cultivated area during the selected growing season is checked using the following procedure
179 (Boschetti et al., 2017): 1) Compare the observed average, maximum, and minimum EVI values
180 with the corresponding thresholds for paddy fields (EVI_{avg_th}, EVI_{max_th}, and EVI_{min_th}) to reduce
181 misclassification problems with evergreen forests and non-vegetative areas; 2) Check for the
182 existence of a maximum inflection point on the EVI curve, which must show a consistent
183 increasing trend before the maxima and a consistent decreasing trend after the maxima. The time
184 interval between the inflection points of the minimum and maximum EVI values during the
185 season must fall within the range of rice vegetative growing periods [$vl1$, $vl2$]; 3) Check if the
186 meteorological conditions on the day of the minimum are favourable for rice crop establishment
187 based on a MODIS-LST value above a specified threshold (LST_{th}); 4) Detect a flood signal (NDFI
188 $\geqslant minndfi$) within a time window ($winfl$) centred on the minimum; 5) Check if there is a
189 consistent increase in EVI observed after the minimum; 6) Check if EVI decreases by more than
190 *decrth*% of the amplitude of the min-max range in a time window after the maxima ($windecr$).
191 Only if all the above requirements are satisfied, the selected growing season in the pixel is

192   labelled as a rice season. The PhenoRice parameters used in the study were calibrated by the
193   phenological observations from the AMSs in China (Table 1).

194   ③ **Estimate rice planting, flowering, and maturity dates**: The rice calendar dates were estimated
195   in the detected rice pixels within the rice seasons. On the EVI time-series curve, the onset date of
196   the field growth period corresponds to the date of the minimum point closest to the retained
197   maximum; the flowering date corresponds to the mid-point date of the period during which the
198   EVI smoothed signal remains above the 90th percentile of the min-max range; the maturity date
199   corresponds to the date when the EVI declined by *decrth*% of the amplitude of the min-max range.
200   Additionally, the study categorized the detected rice calendars into early, middle, and late seasons
201   based on the following rules: 1) the rice with a transplanting date of DOY30-130 and a growing
202   period of 70–100 days was defined as early-season rice; 2) the rice with a transplanting date of
203   DOY110–180 and a growing period of 100–130 days was defined as middle-season rice; 3) the
204   rice with a transplanting date of DOY150-230 and a growing period of 130-150 days was defined
205   as late-season rice.

206   **2.3.3   Data validation**

207   We validated the extracted rice areas during 2003-2020 against the statistics from agricultural
208   yearbooks at the province level. The Chinese Agricultural Yearbooks classify rice varieties into three
209   categories: ER (early rice), MR-SLR (middle rice and single-season late rice), and DLR (double-season
210   late rice). For the consistency of our rice area data with the statistics in variety categorization, we
211   calculated rice planting frequency at the village level and differentiated late rice into single-season late
212   rice and double-season late rice. Due to the difference in spatial resolution between ChinaRiceCalendar
213   and ChinaCropPhen1km, we selected the rice pixels of ChinaRiceCalendar within a one-kilometer
214   radius of the AMSs and the rice pixels of ChinaCropPhen1km within a four-kilometer radius of the
215   AMSs to compare the mean cropping dates in these rice pixels with the corresponding AMS data. Two
216   criteria were used to evaluate the accuracy of the estimated rice areas and cropping dates in each season,
217   namely Root Mean Squared Error (RMSE, Eq. (2)) and R^2 (Eq. (3)):

$$RMSE = \sqrt{\frac{1}{N}\sum_{i=1}^{N}(true_i - est_i)^2} \tag{2}$$

$$R^2 = \left(\frac{\sum_{i=1}^{N}(est_i - \overline{est})(true_i - \overline{true})}{\sqrt{\sum_{i=1}^{N}(est_i - \overline{est})^2}\sqrt{\sum_{i=1}^{N}(true_i - \overline{true})^2}}\right)^2 \tag{3}$$

220   where $true_i$ is the true value in the ith province or AMS; est_i is the corresponding estimated value;
221    $\overline{est}$ and $\overline{true}$ denote the mean of the estimated and true values, respectively; N is the number of
222   provinces or AMSs.

223

224   Additionally, in order to investigate the historical shifts of rice phenological dates in China, we
225   analyzed the trends of rice planting, flowering, and maturity dates at the county level by a
226   Sen+Mann-Kendall trend analysis at a significance level of 0.05. The trend analysis method is detailed
227   in Gocic et al. (2013) .

3   Result

3.1   Validation of rice areas

The detected rice areas during 2003-2020 show a good agreement with statistical sown areas of rice in various growing seasons (Fig. 3). The R^2 between the detected and statistical areas of ER, MR-SLR, and DLR at the province level is 0.92, 0.83, and 0.85, respectively. The RMSE between the detected and statistical areas of ER, MR-SLR, and DLR at the province level is 127.86, 313.06, and 197.47 kha, respectively. The R^2 between the detected and statistical rice areas in different agricultural regions is shown in Table 2. Early rice is mainly distributed in the MLY, SC, SCS, and YGP regions in China and all four regions show high accuracy ($R^2 \in [0.89, 0.97]$) in the detected area of early rice. The NP, HP, and LP regions show higher accuracy ($R^2 \in [0.93, 0.95]$) than the SCS, MLY, SC, and YGP regions ($R^2 \in [0.73, 0.82]$) in the detected area of middle rice and single-season late rice. Moreover, the MLY and YGP regions have more reliable data ($R^2 \in [0.85, 0.89]$) on the area of double-season late rice than the SC and SCS regions ($R^2 \in [0.78, 0.79]$).

3.2   Validation of rice calendars

Overall, the key phenological dates estimated in the study show high consistency with the data from AMSs (Fig. 4). The R^2 between data from ChinaRiceCalendar and AMSs for transplanting, flowering, and maturity dates in China is 0.95, 0.95, and 0.96, respectively. The RMSE between data from ChinaRiceCalendar and AMSs for transplanting, flowering, and maturity dates in China is 8.34, 7.84, and 7.77 days, respectively. Moreover, the error in detected middle-rice calendars is lower than that in early-rice and late-rice calendars (Fig. 4). The RMSE of the estimated transplanting, flowering, and maturity dates for early rice is 8.82, 8.27, and 10.77 days, respectively. The RMSE of the estimated transplanting, flowering, and maturity dates for middle rice is 7.44, 6.53, and 5.14 days, respectively. The RMSE of the estimated transplanting, flowering, and maturity dates for late rice is 8.28, 9.07, and 10.06 days, respectively.

Also, we calculated the RMSE of the estimated rice cropping dates in the seven agricultural regions in China (Fig. 5). Except in the SC region, the RMSE averages of the estimated phenological dates are around one week at the regional scale. For early-season rice, the RMSE average of the estimated cropping dates is 6.76, 13.54, and 7.30 days in the MLY, SC, and YGP, respectively. For middle-season rice, the range of the RMSEs in the seven agricultural regions is from 5.46 days in the NP to 7.81 days in the SC. For late-season rice, the RMSE average of the estimated cropping dates is 8.60, 10.08, and 8.29 days in the MLY, SC, and YGP, respectively.

3.3   Comparison with other calendar datasets

The rice phenological dates obtained from the RiceAtlas (Laborte et al., 2017), ChinaCropPhen1km (Luo et al., 2020), and RICA (Mishra et al., 2021) datasets were also validated against the spatially corresponding AMS data. In China, the rice phenological dates estimated in ChinaRiceCalendar show higher accuracy by growing season than those obtained from RiceAtlas and RICA. Furthermore, compared to the ChinaCropPhen1km dataset, the ChinaRiceCalendar dataset have similar accuracy in rice phenological dates but higher accuracy in rice areas in different growing seasons.

The RMSE between RiceAtlas' and AMSs' phenological dates for early, middle, and late rice in China is 18.27, 21.03, and 13.81 days, respectively. The R^2 between RiceAtlas' and AMSs' phenological dates for early, middle, and late rice in China is 0.65, 0.43, and 0.75, respectively.

The RMSE between ChinaCropPhen1km's and AMSs' phenological dates is 9.35 days for early and middle rice, and 7.24 days for late rice in China. The R^2 between ChinaCropPhen1km's and AMSs' phenological dates is 0.81 for early and middle rice, and 0.85 for late rice in China.

The RMSE between RICA's and AMSs' phenological dates for early, middle, and late rice in China is 22.80, 14.07, and 13.61 days, respectively. The R^2 between RICA's and AMSs' phenological dates for early, middle, and late rice in China is 0.47, 0.69, and 0.73, respectively.

3.4   Spatial distribution of rice areas and phenological dates

According to the spatial distribution of the detected rice areas during 2003-2020, early and late rice were mainly grown in the southern part of China, while middle rice was widely planted in China from south to north (Fig. 6). Based on the mean values between 2003 and 2020, the detected planting area of early rice in China was 4732 kha, and approximately 69% of the early-rice area was concentrated in the MLY region; the detected planting area of middle rice in China was 13953 kha, and approximately 85% of the middle-rice area was distributed in the MLY, NP, and SCS regions; the detected planting area of single-season late rice in China was 4361 kha, and approximately 70% of the single-season late rice area was distributed in the MLY region; the detected planting area of double-season late rice in China was 6423 kha, and approximately 64% of the double-season late rice area was distributed in the MLY region.

The spatial variations of rice phenology are significant in early, middle, and late seasons (Fig. 7 and 8). In the NP, HP, and LP, middle rice was transplanted at DOY130±21, flowered at DOY200±14, and matured at DOY260±14. In the YGP, the mean transplanting date was approximately DOY60 for early rice, DOY125 for middle rice, and DOY150 for late rice; the mean flowering date for early, middle, and late rice was DOY180±30; the mean maturity date was approximately DOY180 for early rice, DOY250 for middle rice, and DOY290 for late rice. In the MLY, the mean transplanting date was approximately DOY110 for early rice, DOY160 for middle rice, and DOY170 for late rice; the mean flowering date was approximately DOY160 for early rice, DOY220 for middle rice, and DOY250 for late rice; the mean maturity date was DOY280±21 for the three seasons. In the SC, the mean transplanting date was approximately DOY90 for early rice and DOY180 for late rice; the mean flowering date was approximately DOY180 for early rice and DOY240 for late rice; the mean maturity date was approximately DOY210 for early rice and DOY300 for late rice.

3.5   Temporal changes in rice phenological dates

Based on the trend analysis of rice phenological dates from 2003 to 2020 (Fig. 9), the transplanting dates for early, middle, and late rice shifted by +5.4, +2.6, and -5.7 DOY/decade, respectively; the flowering date for early, middle, and late rice shifted by +5.5, -2.8, and -2.7 DOY/decade, respectively;

the maturity date for early, middle, and late rice shifted by +3.2, -3.6, and -5.1 DOY/decade, respectively. According to the trend analysis result in each rice-producing county in China between 2003 and 2020 (Fig. 10), 27%, 12%, and 3% of the counties showed a significant delay in transplanting dates for early, middle, and late rice, respectively; meanwhile, 5%, 6%, and 25% of the counties showed a significant advancement in transplanting dates for early, middle, and late rice, respectively. Moreover, 27%, 9%, and 1% of the counties in China showed a significant delay in flowering dates for early, middle, and late rice, respectively; meanwhile, 1%, 7%, and 22% of the counties showed a significant advancement in flowering dates for early, middle, and late rice, respectively. Also, 24%, 6%, and 2% of the counties in China showed a significant delay in maturity dates for early, middle, and late rice, respectively; meanwhile, 2%, 14%, and 19% of the counties showed a significant advancement in flowering dates for early, middle, and late rice, respectively. Overall, the growing season of early rice tended to be delayed, while the growing season of late rice tended to advance between 2003 and 2020 in China. Additionally, the shifts in the phenological dates of middle rice during 2003-2020 depended on the agricultural region (Fig. 10).

4 Uncertainties in ChinaRiceCalendar

Although the generated dataset ChinaRiceCalendar shows an advantage in rice season identification, there is still uncertainty in the data source and phenology detection methods.

This study used MODIS remote sensing data to extract rice phenological dates in various growing seasons in China. The MODIS remote sensing products have an appropriate temporal resolution, long time series, and good time consistency for analyzing changes in rice calendars at the regional scale. Moreover, the MODIS data are easy to obtain and process on the GEE platform, allowing for automated and timely updating of the calendar dataset. However, the pixel-based detection of rice areas may be interfered with by the contamination of clouds, aerosols, and water vapor, especially during the monsoon season when rice is by far the dominant crop (Xiao et al., 2014; Mishra et al., 2021). Because synthetic aperture radar (SAR) can penetrate through clouds, subsequent studies could combine optical and SAR images to avoid the impacts of clouds (Shen et al., 2023). Also, most paddies in southern China are smaller than the spatial resolution of MODIS data, which may result in a rough estimation of rice areas. Generating more satellite remote sensing products with higher spatial resolution and integrating multiple data sources from satellite-airborne-ground observations will facilitate real-time monitoring of rice cropping areas at the regional scale (Zheng et al., 2022; Sun et al., 2023). Additionally, precisely corresponding the image pixels from the MODIS dataset to the Agricultural Meteorological Stations remains a challenge during data validation. In the future, it would be beneficial to conduct a quantitative assessment to determine the representativeness of the MODIS pixels surrounding the AMS site.

In this study, we improved the method of growing season division in the PhenoRice algorithm. We also attempted to remove non-paddy pixels and reduce the impacts of low-quality data on the reconstruction of EVI time-series curves. Nevertheless, since the PhenoRice algorithm detects rice pixels by agronomic flooding signals, rainfed or upland rice systems will be much harder to detect. In China, rice is mainly planted in flooded paddy fields (Luo et al., 2022), which mitigates the problems of detecting rainfed or upland rice. Moreover, the VI-curve smoothing methods perform differently in different

regions (Luo et al., 2020). To enhance the identification of rice growing seasons in multi-cropping areas, we suggested identifying the optimal smoothing method for MODIS-EVI time series in various rice-based cropping systems. Although the local tuning of the PhenoRice algorithm parameters could further improve the results, we employed a single configuration of temporal windows and threshold values across China because automated methods that perform robustly are essential for developing timely information about crop calendars over large extents (Mishra et al., 2021).

The uncertainty in crop area estimation is more significant for late rice than for early and middle rice, resulting in lower accuracy of the detected rice area in southern China (MLY, SC, SCS, YGP) than in northern China (NP, HP, LP). For example, there is an underestimation of the double-season late rice area in Hainan Province and an overestimation of the single-season late rice area in Hubei Province. Because the transplanting dates (DOY150-210) of late rice coincide with the rainy season in the main rice-producing areas, there is a higher risk of misidentifying agronomic flooding signals during transplanting for late rice than for early and middle rice. Furthermore, low data quality induced by cloud contamination during the transplanting period contributes to the difficulties in extracting the late rice area (Xiao et al., 2005; Clauss et al., 2016). Also, the diverse multi-cropping systems and the complex growing environments (e.g., topography and landscape) make the area detection for late rice more challenging (Dong and Xiao, 2016). The following study could consider utilizing geostationary satellite observations to increase the temporal frequency of remote sensing data during the transplantation period of late rice in China (Shen et al., 2023). Subsequently, we will try to automate the generation of ChinaRiceCalendar based on the 'rgee' package (Aybar et al., 2023) and update the database once a year.

5   Data Availability

ChinaRiceCalendar is a raster dataset with 250m, 1km, and 10km spatial resolution. The spatial reference system of the dataset is Asia_North_Albers_Equal_Area_Conic. The dataset currently covers the following periods: 2003-2010, 2011-2015, and 2016-2020. ChinaRiceCalendar is available at https://doi.org/10.7910/DVN/EUP8EY (Hui Li, 2023).

6   Conclusions

In the study, we improved the procedure of growing season division in the PhenoRice algorithm, and detected rice areas and rice phenology in early, middle, and late seasons across China from 2003 to 2020. Then, we established a multi-season rice calendar dataset named ChinaRiceCalendar. Firstly, the detected rice areas in ChinaRiceCalendar show a good agreement with statistical sown areas of rice in various growing seasons. The R^2 between the detected and statistical areas of ER, MR-SLR, and DLR at the province level is 0.92, 0.83, and 0.85, respectively. Secondly, the key phenological dates in ChinaRiceCalendar have high consistency with the field observations from 338 Agricultural Meteorological Stations in China. The RMSE between data from ChinaRiceCalendar and AMSs for rice transplanting, flowering, and maturity dates in China is 8.34, 7.84, and 7.77 days, respectively. Thirdly, ChinaRiceCalendar shows higher accuracy in the detected rice area or key phenological dates by growing season than RiceAtlas, ChinaCropPhen1km, and RICA in China. According to the calendar

data from 2003 to 2020, the transplanting dates for early, middle, and late rice shifted by +5.4, +2.6, and -5.7 DOY/decade, respectively; the flowering date for early, middle, and late rice shifted by +5.5, -2.8, and -2.7 DOY/decade, respectively; the maturity date for early, middle, and late rice shifted by +3.2, -3.6, and -5.1 DOY/decade, respectively. Overall, ChinaRiceCalendar provides more reliable data to investigate and optimize the spatio-temporal structure of rice cultivation in China under climate and land-use change.

Author Contributions: Conceptualization, methodological and algorithmic improvements, HL and XW; data download and processing, YL and ZL; validation, SC and QW; formal analysis, HL, XW, and TZ; writing-original draft preparation, HL and XW; writing-review and editing, XW, SW and LW. All authors have read and agreed to the published version of the manuscript.

Financial support: This research has been supported by the National Natural Science Foundation of China (Project Nos. 31861143015 and 32301393).

Acknowledgments: We would like to thank Dongdong Kong from China University of Geosciences (Wuhan) for providing the R package *Phnofit* and thank Mirco Boschetti from the Italian National Research Council for providing the source code of *PhenoRice*.

Conflicts of Interest: The authors declare no conflict of interest.

References

Atzberger, C. and Eilers, P.H.: Evaluating the effectiveness of smoothing algorithms in the absence of ground reference measurements. International Journal of Remote Sensing, 32(13), 3689-3709, 2011.

Aybar, C. rgee: R Bindings for Calling the 'Earth Engine' API (Version 1.1.7). https://github.com/r-spatial/rgee/issues/, 2023.

Bai, H. and Xiao, D.: Spatiotemporal changes of rice phenology in China during 1981 – 2010. Theoretical and Applied Climatology, 140, 1483-1494, 2020.

Boschetti, M., Busetto, L., Manfron, G., Laborte, A., Asilo, S., Pazhanivelan, S. and Nelson, A.: PhenoRice: A method for automatic extraction of spatio-temporal information on rice crops using satellite data time series. Remote sensing of environment, 194, 347-365, 2017.

Boschetti, M., Stroppiana, D., Brivio, P. and Bocchi, S.: Multi-year monitoring of rice crop phenology through time series analysis of MODIS images. International journal of remote sensing, 30(18), 4643-4662, 2009.

Busetto, L., Zwart, S.J. and Boschetti, M.: Analysing spatial – temporal changes in rice cultivation practices in the Senegal River Valley using MODIS time-series and the PhenoRice algorithm. International Journal of Applied Earth Observation and Geoinformation, 75, 15-28, 2019.

Bush, E.R., Abernethy, K.A., Jeffery, K., Tutin, C., White, L., Dimoto, E., Dikangadissi, J.T., Jump, A.S. and Bunnefeld, N.: Fourier analysis to detect phenological cycles using long‑term tropical field data and simulations. Methods in Ecology and Evolution, 8(5), 530-540, 2017.

Cao, J., Cai, X., Tan, J., Cui, Y., Xie, H., Liu, F., Yang, L. and Luo, Y.: Mapping paddy rice using Landsat time series data in the Ganfu Plain irrigation system, Southern China, from 1988－ 2017. International Journal of Remote Sensing, 42(4), 1556-1576, 2021.

Carleton, T.A.: Crop-damaging temperatures increase suicide rates in India. Proceedings of the National Academy of Sciences, 114(33), 8746-8751, 2017.

Clauss, K., Yan, H. and Kuenzer, C.: Mapping paddy rice in China in 2002, 2005, 2010 and 2014 with MODIS time series. Remote Sensing, 8(5), 434, 2016.

Dong, J. and Xiao, X.: Evolution of regional to global paddy rice mapping methods: A review. ISPRS Journal of Photogrammetry and Remote Sensing, 119, 214-227, 2016.

Fahad, S., Adnan, M., Noor, M., Arif, M., Alam, M., Khan, I.A., Ullah, H., Wahid, F., Mian, I.A. and Jamal, Y.: Major constraints for global rice production, Advances in rice research for abiotic stress tolerance. Elsevier, pp. 1-22, 2019.

Franke, J.A., Müller, C., Elliott, J., Ruane, A.C., Jägermeyr, J., Snyder, A., Dury, M., Falloon, P.D., Folberth, C. and François, L.: The GGCMI Phase 2 emulators: global gridded crop model responses to changes in CO_2, temperature, water, and nitrogen (version 1.0). Geoscientific Model Development, 13(9), 3995-4018, 2020.

Fritz, S., See, L., Bayas, J.C.L., Waldner, F., Jacques, D., Becker-Reshef, I., Whitcraft, A., Baruth, B., Bonifacio, R. and Crutchfield, J.: A comparison of global agricultural monitoring systems and current gaps. Agricultural systems, 168, 258-272, 2019.

Frolking, S., Qiu, J., Boles, S., Xiao, X., Liu, J., Zhuang, Y., Li, C. and Qin, X.: Combining remote sensing and ground census data to develop new maps of the distribution of rice agriculture in China. Global Biogeochemical Cycles, 16(4), 38-1-38-10, 2002.

Gao, F. and Zhang, X.: Mapping crop phenology in near real-time using satellite remote sensing: Challenges and opportunities. Journal of Remote Sensing, 2021, 2021.

Gocic, M. and Trajkovic, S.: Analysis of changes in meteorological variables using Mann-Kendall and Sen's slope estimator statistical tests in Serbia. Global and Planetary Change, 100, 172-182, 2013.

Gumma, M.K., Nelson, A., Thenkabail, P.S. and Singh, A.N.: Mapping rice areas of South Asia using MODIS multitemporal data. Journal of applied remote sensing, 5(1), 053547, 2011.

Guo, L., An, N. and Wang, K.: Reconciling the discrepancy in ground－and satellite－observed trends in the spring phenology of winter wheat in China from 1993 to 2008. Journal of Geophysical Research: Atmospheres, 121(3), 1027-1042, 2016.

Han, J., Zhang, Z., Luo, Y., Cao, J., Zhang, L., Zhuang, H., Cheng, F., Zhang, J. and Tao, F.: Annual paddy rice planting area and cropping intensity datasets and their dynamics in the Asian monsoon region from 2000 to 2020. Agricultural Systems, 200, 103437, 2022.

He, Y., Dong, J., Liao, X., Sun, L., Wang, Z., You, N., Li, Z. and Fu, P.: Examining rice distribution and cropping intensity in a mixed single-and double-cropping region in South China using all available Sentinel 1/2 images. International Journal of Applied Earth Observation and Geoinformation, 101, 102351, 2021.

Hui Li, Xiaobo Wang, Shaoqiang Wang, Yuanyuan Liu, Zhenhai Liu, Shiliang Chen, Qinyi Wang, Tongtong Zhu, Lunche Wang, Lizhe Wang. ChinaRiceCalendar. Harvard Dataverse, doi/10.7910/DVN/EUP8EY, 2023.

IPCC. Climate change 2022: impacts, adaptation and vulnerability. https://www.ipcc.ch/report/sixth-assessment-report-working-group-ii/, 2022.

Kim, D.-H., Jang, T., Hwang, S., and Jeong, H.: Paddy rice adaptation strategies to climate change: Transplanting date shift and BMP applications, Agricultural Water Management, 252, 106926, 2021.

Kong, D., McVicar, T.R., Xiao, M., Zhang, Y., Peña‐Arancibia, J.L., Filippa, G., Xie, Y. and Gu, X.: phenofit: An R package for extracting vegetation phenology from time series remote sensing. Methods in Ecology and Evolution, 2022.

Kotsuki, S. and Tanaka, K.: SACRA – a method for the estimation of global high-resolution crop calendars from a satellite-sensed NDVI. Hydrology and Earth System Sciences, 19(11), 4441-4461, 2015.

Laborte, A.G., Gutierrez, M.A., Balanza, J.G., Saito, K., Zwart, S.J., Boschetti, M., Murty, M., Villano, L., Aunario, J.K. and Reinke, R.: RiceAtlas, a spatial database of global rice calendars and production. Scientific data, 4(1), 1-10, 2017.

Liu, L., Huang, J., Xiong, Q., Zhang, H., Song, P., Huang, Y., Dou, Y. and Wang, X.: Optimal MODIS data processing for accurate multi-year paddy rice area mapping in China. GIScience & Remote Sensing, 57(5), 687-703, 2020.

Liu, Y., Zhou, W. and Ge, Q.: Spatiotemporal changes of rice phenology in China under climate change from 1981 to 2010. Climatic Change, 157, 261-277, 2019.

Luo, W., Chen, M., Kang, Y., Li, W., Li, D., Cui, Y., Khan, S. and Luo, Y.: Analysis of crop water requirements and irrigation demands for rice: Implications for increasing effective rainfall. Agricultural Water Management, 260, 107285, 2022.

Luo, Y., Zhang, Z., Chen, Y., Li, Z. and Tao, F.: ChinaCropPhen1km: a high-resolution crop phenological dataset for three staple crops in China during 2000–2015 based on leaf area index (LAI) products. Earth System Science Data, 12(1), 197-214, 2020.

Mishra, B., Busetto, L., Boschetti, M., Laborte, A. and Nelson, A.: RICA: A rice crop calendar for Asia based on MODIS multi year data. International Journal of Applied Earth Observation and Geoinformation, 103, 102471, 2021.

More, R.S., Manjunath, K., Jain, N.K., Panigrahy, S. and Parihar, J.S.: Derivation of rice crop calendar and evaluation of crop phenometrics and latitudinal relationship for major south and south-east Asian countries: A remote sensing approach. Computers and Electronics in Agriculture, 127, 336-350, 2016.

Nelson, A. and Gumma, M.: A map of lowland rice extent in the major rice growing countries of Asia. IRRI, Los Banos, Philippines, 2015.

Pan, Z., Huang, J., Zhou, Q., Wang, L., Cheng, Y., Zhang, H., Blackburn, G.A., Yan, J. and Liu, J.: Mapping crop phenology using NDVI time-series derived from HJ-1 A/B data. International Journal of Applied Earth Observation and Geoinformation, 34, 188-197, 2015.

503 Parmesan, C., Morecroft, M.D. and Trisurat, Y.: Climate change 2022: Impacts, adaptation and
504 vulnerability, GIEC, 2022.

505 Qiu, J., Tang, H., Frolking, S., Boles, S., Li, C., Xiao, X., Liu, J., Zhuang, Y. and Qin, X.: Mapping
506 single‐, double‐, and triple‐crop agriculture in China at 0.5°× 0.5° by combining county‐scale census
507 data with a remote sensing‐derived land cover map. Geocarto International, 18(2), 3-13, 2003.

508 Reed, B.C., Brown, J.F., VanderZee, D., Loveland, T.R., Merchant, J.W. and Ohlen, D.O.: Measuring
509 phenological variability from satellite imagery. Journal of vegetation science, 5(5), 703-714, 1994.

510 Sakamoto, T., Wardlow, B.D., Gitelson, A.A., Verma, S.B., Suyker, A.E. and Arkebauer, T.J.: A
511 two-step filtering approach for detecting maize and soybean phenology with time-series MODIS data.
512 Remote Sensing of Environment, 114(10), 2146-2159, 2010.

513 Sakamoto, T., Yokozawa, M., Toritani, H., Shibayama, M., Ishitsuka, N. and Ohno, H.: A crop
514 phenology detection method using time-series MODIS data. Remote sensing of environment, 96(3-4),
515 366-374, 2005.

516 Sakamoto, T.: Refined shape model fitting methods for detecting various types of phenological
517 information on major US crops. ISPRS Journal of Photogrammetry and Remote Sensing, 138, 176-192,
518 2018.

519 Shen, R., Pan, B., Peng, Q., Dong, J., Chen, X., Zhang, X., Ye, T., Huang, J. and Yuan, W.:
520 High-resolution distribution maps of single-season rice in China from 2017 to 2022. Earth System
521 Science Data Discussions, 1-27, 2023.

522 Shen, Y., Zhang, X., Yang, Z., Ye, Y., Wang, J., Gao, S., Liu, Y., Wang, W., Tran, K.H. and Ju, J.:
523 Developing an operational algorithm for near-real-time monitoring of crop progress at field scales by
524 fusing harmonized Landsat and Sentinel-2 time series with geostationary satellite observations. Remote
525 Sensing of Environment, 296, 113729, 2023.

526 Shihua, L., Jingtao, X., Ping, N., Jing, Z., Hongshu, W. and Jingxian, W.: Monitoring paddy rice
527 phenology using time series MODIS data over Jiangxi Province, China. International Journal of
528 Agricultural and Biological Engineering, 7(6), 28-36, 2014.

529 Son, N.-T., Chen, C.-F., Chen, C.-R., Duc, H.-N. and Chang, L.-Y.: A phenology-based classification of
530 time-series MODIS data for rice crop monitoring in Mekong Delta, Vietnam. Remote Sensing, 6(1),
531 135-156, 2013.

532 Sun, C., Zhang, H., Xu, L., Ge, J., Jiang, J., Zuo, L. and Wang, C.: Twenty-meter annual paddy rice
533 area map for mainland Southeast Asia using Sentinel-1 synthetic-aperture-radar data. Earth System
534 Science Data, 15(4), 1501-1520, 2023.

535 Sun, H., Huang, J. and Peng, D.: Detecting major growth stages of paddy rice using MODIS data. J.
536 Remote Sens, 13, 1122-1137, 2009.

537 Waha, K., Müller, C. and Rolinski, S.: Separate and combined effects of temperature and precipitation
538 change on maize yields in sub-Saharan Africa for mid-to late-21st century. Global and Planetary
539 Change, 106, 1-12, 2013.

540 Wang, J., Yu, K., Tian, M. and Wang, Z.: Estimation of rice key phenology date using Chinese HJ-1

541   vegetation index time-series images, 2019 8th International Conference on Agro-Geoinformatics
542   (Agro-Geoinformatics). IEEE, pp. 1-4, 2019.

543   Wang, X., Ciais, P., Li, L., Ruget, F., Vuichard, N., Viovy, N., Zhou, F., Chang, J., Wu, X. and Zhao, H.:
544   Management outweighs climate change on affecting length of rice growing period for early rice and
545   single rice in China during 1991–2012. Agricultural and Forest Meteorology, 233, 1-11, 2017.

546   Wang, X., Folberth, C., Skalsky, R., Wang, S., Chen, B., Liu, Y., Chen, J. and Balkovic, J.: Crop
547   calendar optimization for climate change adaptation in rice-based multiple cropping systems of India
548   and Bangladesh. Agricultural and Forest Meteorology, 315, 108830, 2022.

549   Wang, X., Wang, S., Folberth, C., Skalsky, R., Li, H., Liu, Y. and Balkovic, J.: Limiting global
550   warming to 2° C benefits building climate resilience in rice-wheat systems in India through crop
551   calendar management. Agricultural Systems, 213, 103806, 2024.

552   Wu, Q.: geemap: A Python package for interactive mapping with Google Earth Engine. Journal of
553   Open Source Software, 5(51), 2305, 2020.

554   Xiao, X., Boles, S., Frolking, S., Li, C., Babu, J.Y., Salas, W. and Moore III, B.: Mapping paddy rice
555   agriculture in South and Southeast Asia using multi-temporal MODIS images. Remote sensing of
556   Environment, 100(1), 95-113, 2006.

557   Xiao, X., Boles, S., Liu, J., Zhuang, D., Frolking, S., Li, C., Salas, W. and Moore III, B.: Mapping
558   paddy rice agriculture in southern China using multi-temporal MODIS images. Remote sensing of
559   environment, 95(4), 480-492, 2005.

560   Zeng, L., Wardlow, B.D., Wang, R., Shan, J., Tadesse, T., Hayes, M.J. and Li, D.: A hybrid approach for
561   detecting corn and soybean phenology with time-series MODIS data. Remote Sensing of Environment,
562   181, 237-250, 2016.

563   Zhang, X., Friedl, M.A., Schaaf, C.B., Strahler, A.H., Hodges, J.C., Gao, F., Reed, B.C. and Huete, A.:
564   Monitoring vegetation phenology using MODIS. Remote sensing of environment, 84(3), 471-475,
565   2003.

566   Zhang, Z., Song, X., Tao, F., Zhang, S. and Shi, W.: Climate trends and crop production in China at
567   county scale, 1980 to 2008. Theoretical and Applied Climatology, 123(1), 291-302, 2016.

568   Zhao, C., Liu, B., Piao, S., Wang, X., Lobell, D.B., Huang, Y., Huang, M., Yao, Y., Bassu, S. and Ciais,
569   P.: Temperature increase reduces global yields of major crops in four independent estimates.
570   Proceedings of the National Academy of sciences, 114(35), 9326-9331, 2017.

571   Zhao, H., Yang, Z., Di, L. and Pei, Z.: Evaluation of temporal resolution effect in remote sensing based
572   crop phenology detection studies, International Conference on Computer and Computing Technologies
573   in Agriculture. Springer, pp. 135-150, 2011.

574   Zheng, J., Song, X., Yang, G., Du, X., Mei, X. and Yang, X.: Remote sensing monitoring of rice and
575   wheat canopy nitrogen: A review. Remote Sensing, 14(22), 5712, 2022.

576   Zong, W., Ren, D., Huang, M., Sun, K., Feng, J., Zhao, J., Xiao, D., Xie, W., Liu, S. and Zhang,
577   H.: Strong photoperiod sensitivity is controlled by cooperation and competition among Hd1, Ghd7
578   and DTH8 in rice heading. New Phytologist, 229(3), 1635-1649, 2021.

579
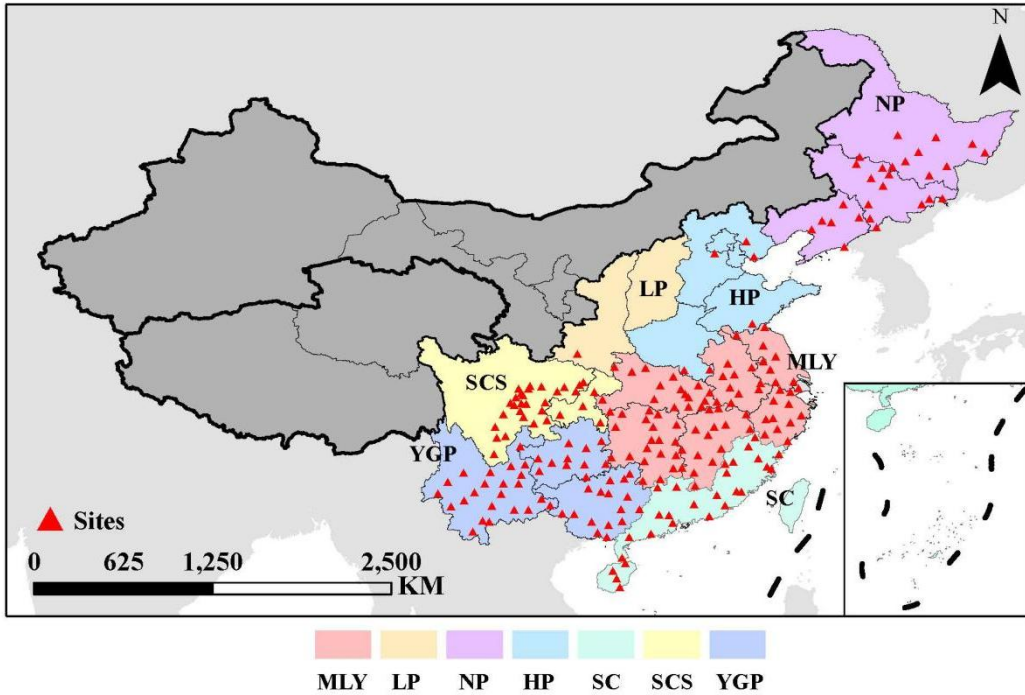
580

581   **Fig.1 Study area and distribution of Agricultural Meteorological Stations (AMSs) in China**

582
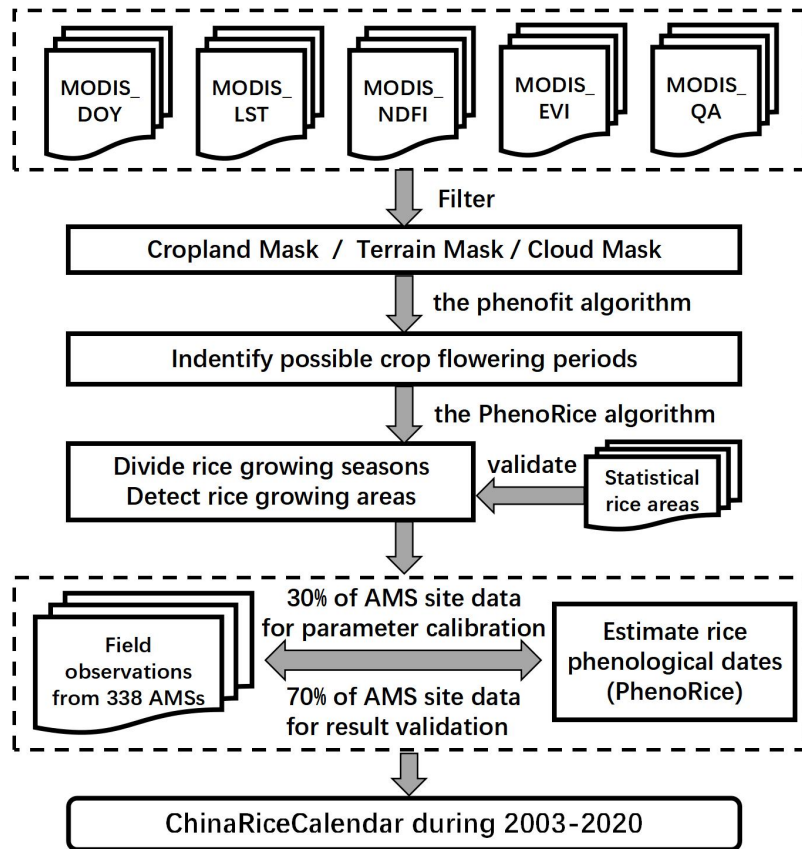
583   **Fig.2 Technology roadmap for this study**

584

585
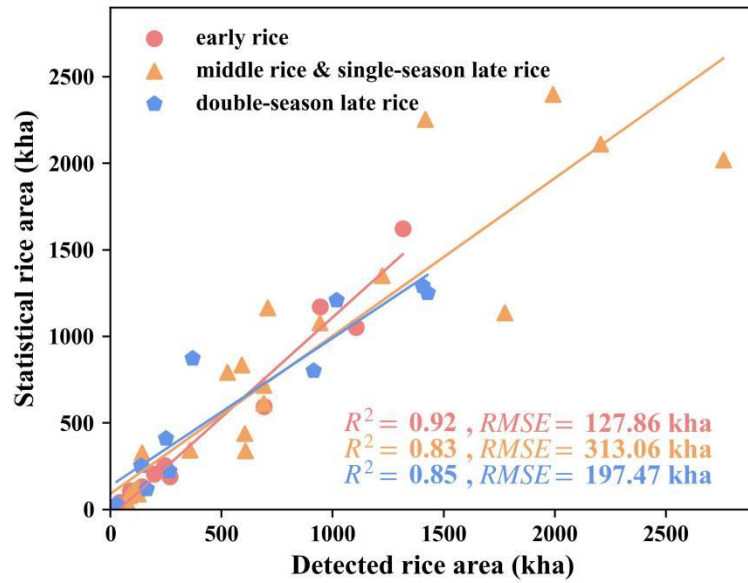
Fig.3 Comparison between detected and statistical rice areas at the province scale (red dots represent early rice, orange squares represent middle rice and single-season late rice, blue pentagons represent double-season late rice)

589
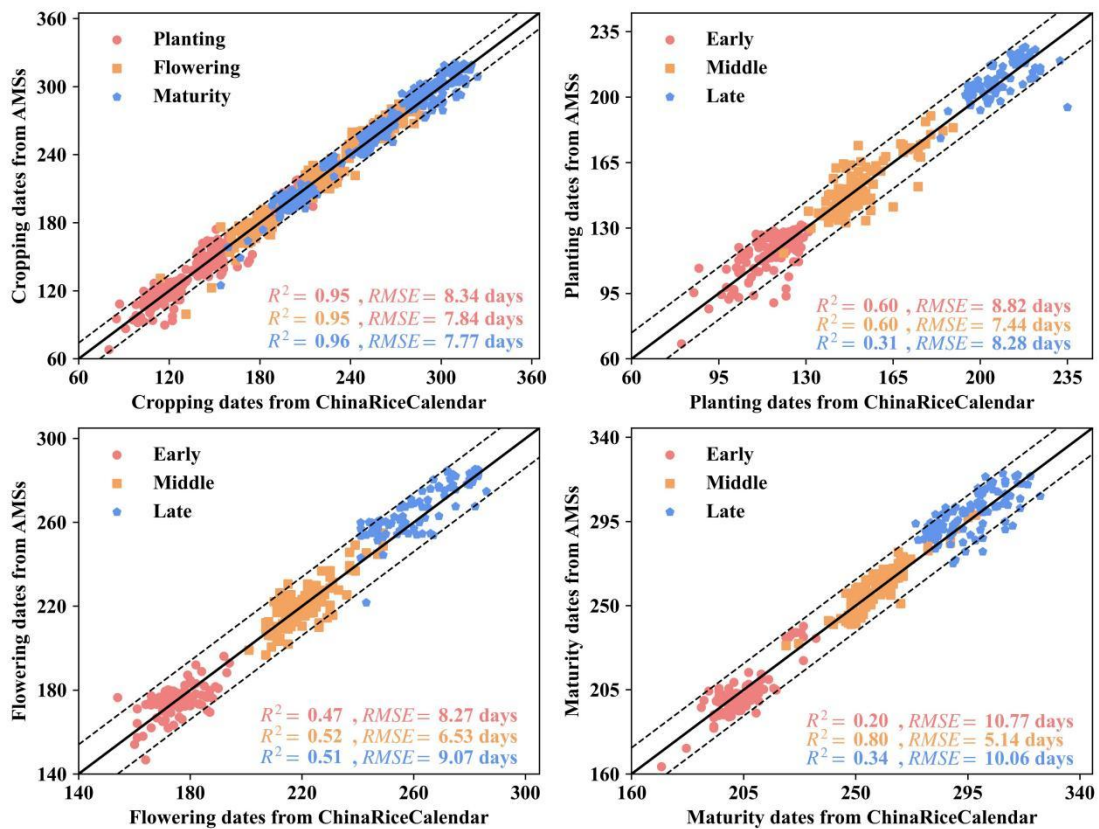
Fig.4 Comparison of rice phenological dates between ChinaRiceCalendar and AMS data at the site scale (dashed lines are ±14 days)
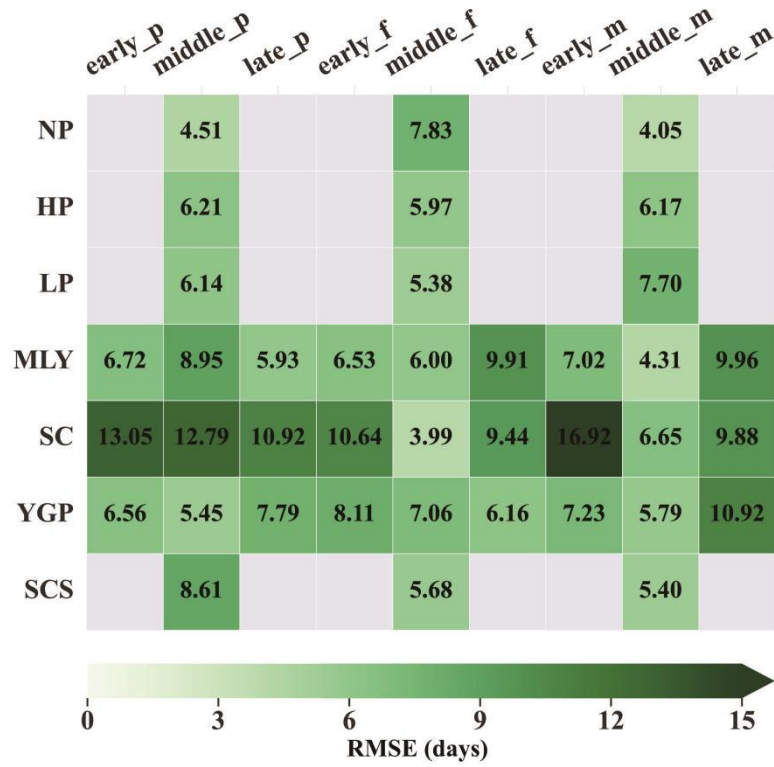
592
Fig.5 RMSEs of rice phenological dates between ChinaRiceCalendar and AMS data in main
agricultural regions

595
596

597
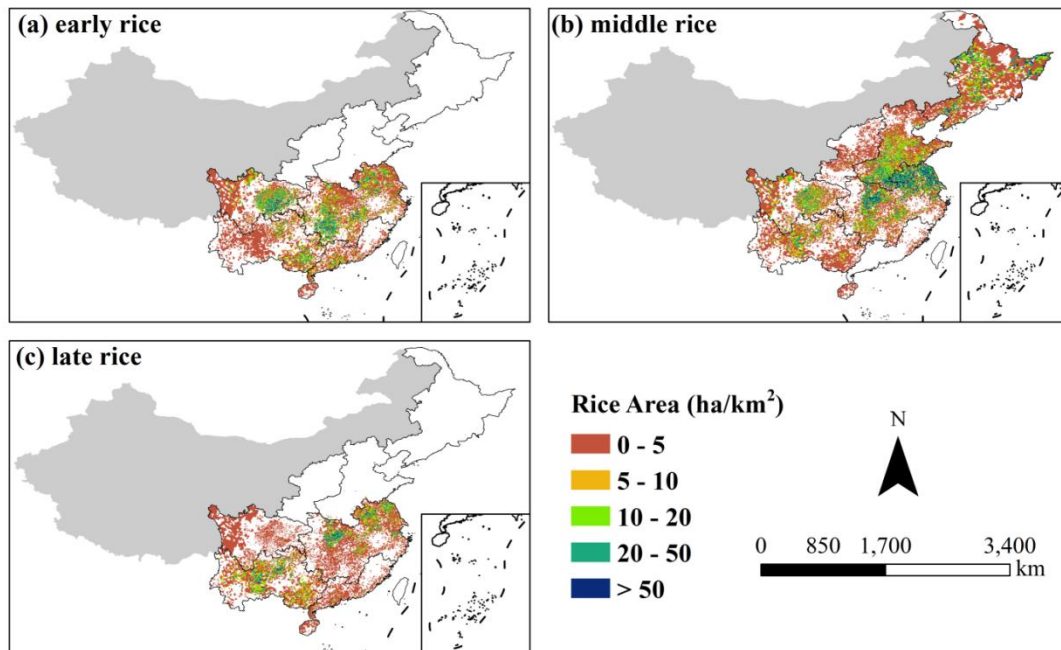
598 **Fig.6 Spatial distribution of rice areas in China during 2003-2020 (a: early rice, b: middle rice, c:**
599 **late rice)**
600

601
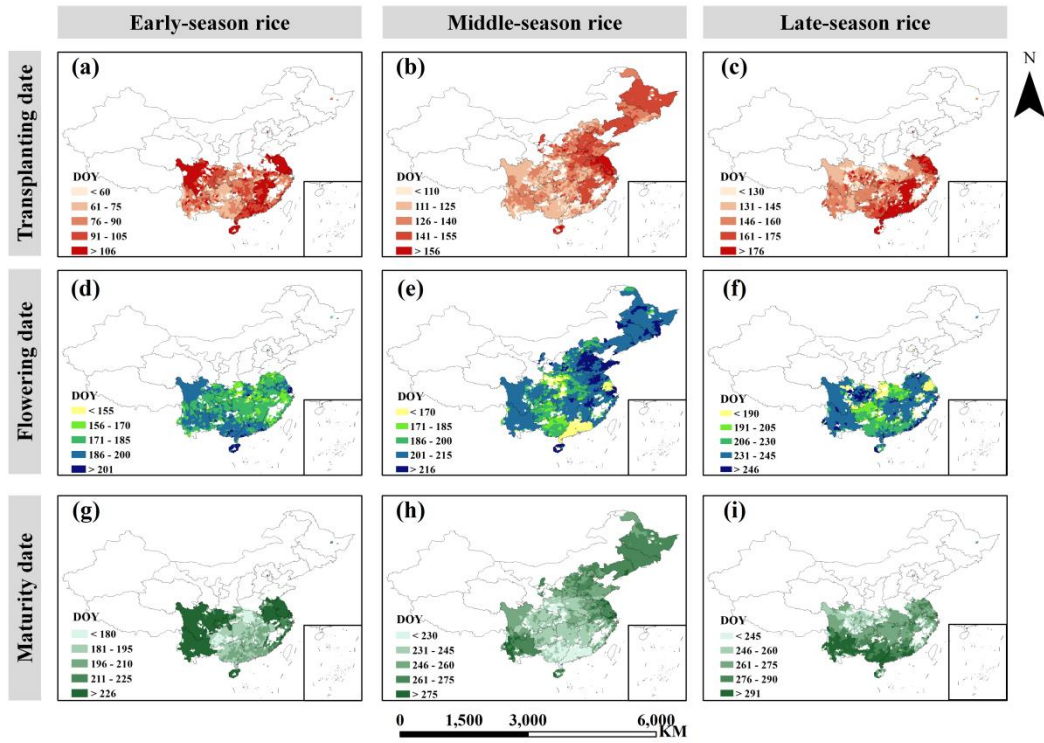
Fig.7 Rice phenological dates at the county scale between 2003 and 2020 (a: early-rice transplanting dates; b: middle-rice transplanting dates; c: late-rice transplanting dates; d: early-rice flowering dates; e: middle-rice flowering dates; f: late-rice flowering dates; g: early-rice maturity dates; h: middle-rice maturity dates; i: late-rice maturity dates)

606
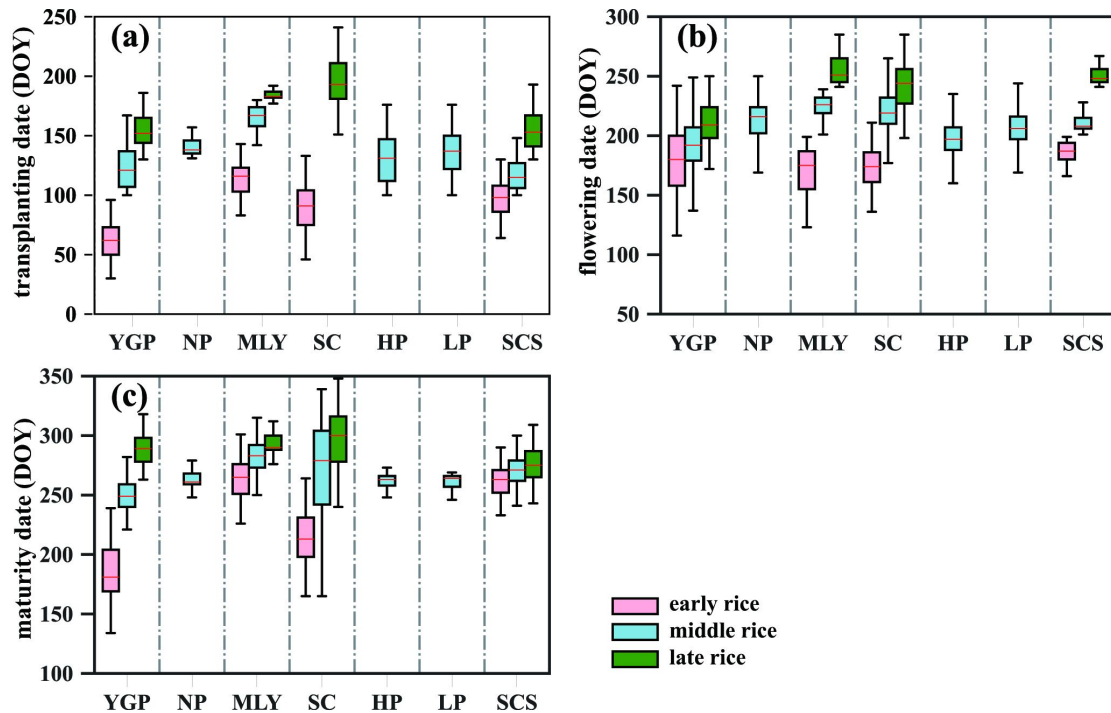
Fig.8 Rice phenological dates in main agricultural regions between 2003 and 2020 (a: Transplanting dates; b: Flowering dates; c: Maturity dates)
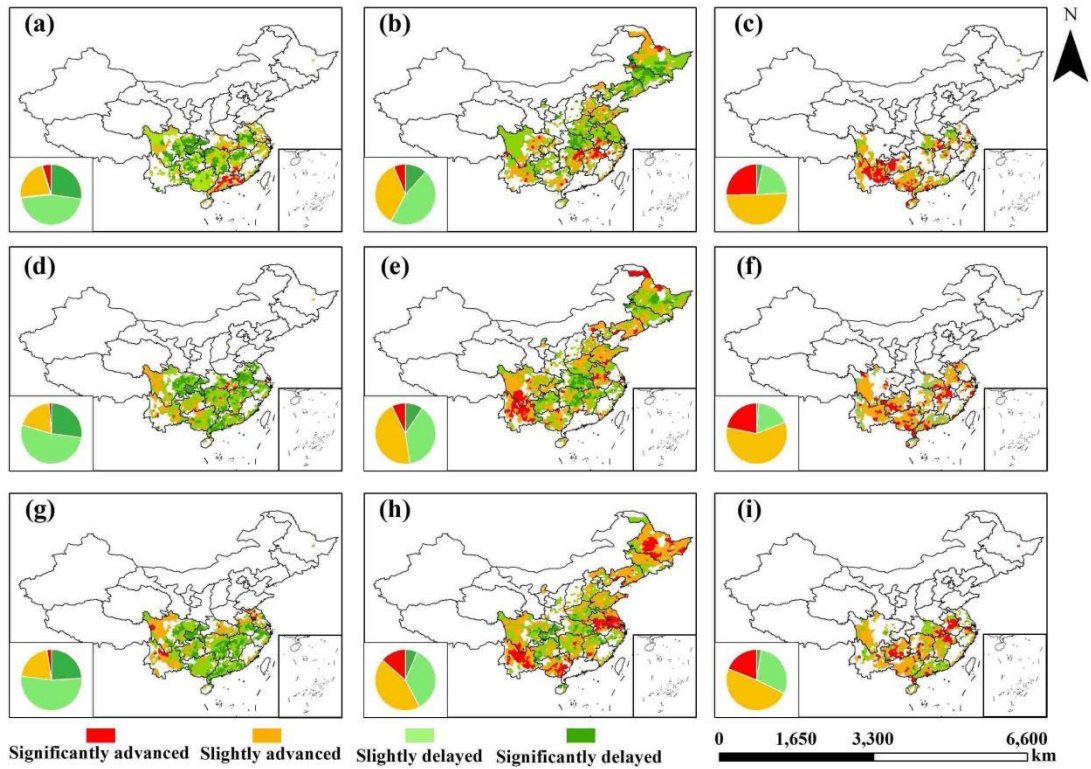
609
610 **Fig.9 Temporal trends in rice phenological dates at the county scale from 2003 to 2020 (a:**
611 **early-rice transplanting dates; b: middle-rice transplanting dates; c: late-rice transplanting dates;**
612 **d: early-rice flowering dates; e: middle-rice flowering dates; f: late-rice flowering dates; g:**
613 **early-rice maturity dates; h: middle-rice maturity dates; i: late-rice maturity dates)**

614

Fig.10 Temporal trends in rice phenological dates at the regional level from 2003 to 2020 (early_p: early-rice transplanting dates; middle_p: middle-rice transplanting dates; late_p: late-rice transplanting dates; early_f: early-rice flowering dates; middle_f: middle-rice flowering dates; late_f: late-rice flowering dates; early_m: early-rice maturity dates; middle_m: middle-rice maturity dates; late_m: late-rice maturity dates)

620

Table.1 PhenoRice parameters used in the study

Parameters	Value	Description
EVI_{avg_th}	0.40	threshold for the average EVI within the study period ($< EVI_{avg\_th}$)
EVI_{max_th}	0.50	threshold for the maximum EVI within the study period ($> EVI_{max\_th}$)
EVI_{min_th}	0.25	threshold for the minimum EVI within the study period ($< EVI_{min\_th}$)
vl1 (days)	40	shortest vegetative growth length
vl2 (days)	112	longest vegetative growth length
tl1 (days)	96	shortest total growth length
tl2 (days)	184	longest total growth length
LST_{th} (ºC)	15	minimum land surface temperature for rice planting
Winfl (days)	24	time window for capturing flooding signals
minndfi	0	threshold for NDFI
Win_{decr} (days)	72	threshold for a decline window after EVI maximum
dec_{th}	0.50	percent decrease of EVI after EVI maximum

621

622

623

624 **Table.2 R^2 between the detected and statistical rice area in main agricultural regions ($p < 0.05$)**

	Early rice	Middle rice & single-season late rice	Double-season late rice
MLY	0.97	0.79	0.85
NP		0.95	
HP		0.94	
SC	0.92	0.73	0.78
LP		0.93	
SCS	0.89	0.82	0.79
YGP	0.90	0.77	0.89

625